



Shahid Chamran  
University of Ahvaz

# Journal of Applied and Computational Mechanics



Research Paper

## Numerical Study of Three-dimensional Boundary-layer Flow over a Wedge: Magnetic Field Analysis

S. Shashi Prabha Gogate<sup>1</sup>, Ramesh B. Kudenatti<sup>2</sup>

<sup>1</sup> Department of Mathematics, M. S. Ramaiah Institute of Technology, Bengaluru-560054, India

<sup>2</sup> Department of Mathematics, Bengaluru Central University, Central College Campus, Bengaluru-560 001, India

Received April 03 2020; Revised June 23 2020; Accepted for publication June 24 2020.

Corresponding author: R.B. Kudenatti (ramesh@bub.ernet.in)

© 2021 Published by Shahid Chamran University of Ahvaz

**Abstract.** The magnetohydrodynamic flow of a viscous fluid over a constant wedge in three-dimensional boundary-layer has been analyzed both numerically and asymptotically. The magnetic field is applied normal to the flow. The mainstream flows aligned with wedge surface are assumed to be proportional to the power of the coordinate distances. The system is described using three-dimensional MHD boundary-layer equations which are converted to couple nonlinear ordinary differential equations using similarity transformations. The resulting equations are solved numerically using the Keller-box method which is second-order accurate and asymptotically for far-field behavior. Both numerical and asymptotic solutions give good agreement in predicting the velocity behaviors and wall shear stresses. The effects of Hartmann number, pressure gradient and shear-to-strain-rate on the velocity fields are studied. Particularly, it is shown that the solutions of three-dimensional boundary-layer for variable pressure gradient exist, its effects are important on the boundary-layer flow. Results show that there are new families of solutions for some range of shear-to-strain-rate and there exists a threshold value of it beyond which no solutions exist. For some range of parameters, there is a reverse flow at which our boundary-layer assumptions are no longer valid. Various results for the velocity profiles, wall-shear stresses and displacement thicknesses are also obtained. The physical mechanisms behind these results are discussed.

**Keywords:** Three-dimensional flow; Wedge flow; Keller-box; Asymptotic; Shear-to-strain-rate; Displacement thickness.

### 1. Introduction

A canonical problem in fluid mechanics concerns about two-dimensional boundary-layer flow in which the velocity components depend on two spatial coordinates, and the viscosity effects are confined near the surface. This gives a good deal of simplifications in the Navier-Stokes equations. The two-dimensional boundary-layer flows, originally developed by Prandtl have significant applications such as aerodynamics, design and analysis of aircraft, boats, submarines, rockets, jet engines, wind turbines, biomedical devices, the cooling of electronic components and the transportation of water, crude oil and natural gases, etc. Although there is a good understanding of two-dimensional boundary-layer flow, an understanding of three-dimensional boundary-layer flow is progressed recently due to its vast applications such as boundary-layer flow over swept wings, turbine bodies, also in biomedical engineering and industries, etc. These flows, in many ways, are linked to a much-complicated flow structure which results into difficult mathematical problems and hence solutions. When solutions exist, they certainly predict interesting flow phenomena and corresponding physical mechanisms. Also, a significant progress in understanding fundamental dynamics of three-dimensional boundary-layer flow has been derived from its two-dimensional analogue (Sowerby [1] and Banks [2]).

An important attempt at describing the three-dimensional flow of a viscous and incompressible fluid was carried out by Davey [3]. In this study was assumed that the outer-mainstream flows were allowed to vary linearly and were irrotational that lead to a stagnation-point flow problem. However, the numerical solutions of the problem were obtained only for  $V_\infty / U_\infty > -1$ , where  $U_\infty$ ,  $V_\infty$  are strain and shear rates, beyond which no solution exists. It was shown by Davey and Schofield [4] that the above three-dimensional boundary-layer problem exists near the two-dimensional stagnation-point by setting  $V_\infty \rightarrow \infty$ . Most of the studies on three-dimensional boundary-layer flows have been restricted to a stagnation point flow. In addition, Davey and Schofield [4] have reported dual solutions of the three-dimensional boundary-layer flow. Recently, Weidman [5] has obtained non-axisymmetric stagnation point flows in three-dimensional boundary-layers in which the outer potential flow is modified by adding periodic and azimuthal velocities, and this leads to a new class of asymmetric stagnation-point flows.

The pressure is supposed to be uniform throughout the flow field i.e. the value of the pressure gradient in the boundary-layer region equals with that of the potential flow, and thus pressure is prescribed by the inviscid flow. In the case of the two-



dimensional, the inviscid flow is one-dimensional whereas, for the three-dimensional boundary-layer flows, it is two-dimensional. In any case, the pressure gradient from the outer inviscid flow is impressed on the boundary-layer with either negative (accelerated flow), zero (the flow over a flat surface) or positive (decelerated flow). Thus, with an appropriately impressed pressure gradient on the boundary-layer, the streamlines are strongly skewed in the viscous boundary-layer than in the inviscid flow. Hirschel et al. [6] studied the three-dimensional boundary-layer flows of the above type usually appear in the context of wing-body junctions. Further, Duck et al. [7] have approximated both outer freestream flows by a power of distance of the form  $x^m$ , where  $x$  is measured along a distance from leading edge and  $m$  is a constant. For zero pressure gradient  $m=0$  similar to the classical Blasius flow, the three-dimensional solution is also possible in which the both velocity profiles have accelerated boundary-layer characters. For  $m=1$ , the details of three-dimensional boundary-layer stagnation-point flow can be found in Rosenhead [8]. Duck and Dry [9] have shown that the similarity-type solutions to the three-dimensional boundary-layer flows do not exist for general values of  $m$ . Thus, these observations provide the motivation for the present investigation.

We will examine the effects of the pressure gradient on the general three-dimensional boundary-layer flows over a wedge surface possessing the velocity profiles in both directions and this work is an extension of the two-dimensional boundary-layer flow and of Duck and Dry [9]. Since the pressure variation is constant along the normal direction ( $z > 0$ ), it is a function of  $x$  and  $y$  along the main flow and secondary flow respectively. The outer freestream flows are characterized by power-law relations (i.e. the outer freestream flows vary as a power of distances along the wedge surfaces) that are proportional to  $x^m$  and  $y^m$ . There are other forms of the power law approximations, see (Hayat et al. [10]). The same  $m$  is taken in both relations because the pressure is uniform quantity in the boundary-layer. Thus, the parameter  $m$  now defines the strength of the pressure gradient and introduces an additional parameter in the boundary-layer equations. When  $m < 0$ , the flow has an adverse pressure gradient i.e. ( $\partial p / \partial x > 0$ ,  $\partial p / \partial y > 0$ ) and for  $m > 0$ , the flow becomes a favorable pressure gradient i.e. ( $\partial p / \partial x < 0$ ,  $\partial p / \partial y < 0$ ). Further, once the self-similar forms are assumed, these power-law relations give a good deal of simplification and lead to discovering a new family of boundary-layer solutions as a function of the shear-to-strain-rate ratio parameter  $\alpha$ . Crucially, it is important to note that although this parameter is absent in two-dimensional flow ( $V_\infty = 0$ ), it does encompass a wide range of three-dimensional boundary-layer flows. In particular, when this parameter  $\alpha$  is negative, the key point is that the secondary flow has a boundary-layer separation only at which power-law assumptions fail. At this point, it is worth to mention that for certain values of  $\alpha$  (say  $\alpha_0$  and is negative), the occurrence of flow separation is common in the  $y$ -direction. This is, however, a function of pressure gradient parameter. By increasing pressure gradient the flow separation could be delayed resulting into decrease the value of  $\alpha_0$  and at the same time solution domain also increases (Hirschel [6]).

On the other hand, the boundary-layer separation could be prevented by including the external forces on the boundary-layer flow. One option is to include the MHD effects on the boundary-layer flow in which it is applied normal to flow directions ( $x$ - and  $y$ -directions). This applied force naturally prevents the flow separation by releasing more energy to the flow. This applied magnetic field certainly removes the decelerated fluid particles present in the flow, thereby making the fluid to attain accelerated flow. Also, the applied magnetic field strictly balances the flow oscillations (Oskam and Veldman [11]) in the boundary layer and has stabilizing effects on three-dimensional flow disturbances (Sommeria and Moreau [12]). Besides this, on the other hand, when the outer freestream velocities are reduced to zero and the wedge is allowed to stretch along its own plane, then this model is described using a three-dimensional laminar boundary layer flow over a stretching surface. In this case, the boundary-layers grow upstream from the leading edge. This model is quite delicate by the fact that the stretching rate needs to be managed and small enough so that the sheet should not break and be flat throughout. This can effectively be done by applying the magnetic field normal to the surface in which it is stretched. In this context, a certain amount of effort has been directed to study the MHD effects on the boundary-layer flow in general, and in particular, the nature of the velocity profiles, although MHD greatly complicates the problem by the fact that the flow is three-dimensional. Allowing the outer freestream velocity to grow linearly in both co-ordinates, Takhar et al. [13] have studied three-dimensional laminar boundary-layer flow when the magnetic field is applied normal to the flow. Also, Hayat et al. [14] studied the magneto hydrodynamic three-dimensional flow of a viscous fluid over a stretching sheet in a porous medium. Ishak et al. [15] have considered magnetic boundary layer flow due to moving extensible surfaces in which the surface is stretched in a uniform manner. To this end, the present work is also devoted to investigating the MHD effects on three-dimensional boundary-layer flows considering a variable pressure gradient, in which the boundary-layers grow downstream from the leading edge at which boundary-layers first form. Awaludin et al. [16] have studied the stability of MHD boundary layer flow and heat transfer and showed that the model shows a dual solution structure for the same set of physical parameters in which the additional solution is always leads to unstable and hence practically cannot be encountered. Recently, Singh et al. [17] have obtained analytical-type solution to the MHD boundary layer flow due to stretching sheet which is embedded in the porous medium.

Thus, the variety of meaningful comparisons between theoretical predictions and experimental observations has led to developing rational mathematical analysis of the three-dimensional model. We will study the effects of the variable pressure gradient and applied magnetic field on general three-dimensional boundary-layer flows. These two parameters alter the nature of the boundary-layer flow but complicate the problem and have been the subject of much interest. These effects lead to several ideas mentioned above including boundary-layer separation. Thus, the equations describing this boundary-layer flow can be derived from Prandtl's equations, Maxwell's equations, Ohm's law, Faraday's law and admit similarity type solutions. These equations are justifiable on the basis of the large Reynolds number, but give all solutions that are independent of Reynolds number. Both numerical and asymptotic methods are presented for tackling various aspects of the problem. In most of the boundary-layer computations, as commonly employed, the finite-difference based Keller-box method which is second-order accurate is used. This method is particularly useful because it allows adopting a variable grid size during the computations (Keller [18]).

The presentation of the paper proceeds as follows. In §2 we derive the problem under discussion including various governing equations, the similarity transformations, etc. The solution procedure by the Keller-box method is discussed in detail in §3. The special case  $m=1$  and  $M=0$  is considered which corresponds to the stagnation point flow (Davey [3] and Rosenhead [8]) in three-dimensional boundary-layers. For other values of these parameters a new class of solutions is obtained and are analyzed. Section 4 devotes to assess the results obtained for  $m$ ,  $M$  and  $\alpha$  (including large  $\alpha$ ) by taking large  $\alpha$  asymptotics of the problem. For large  $\alpha$ , the regular perturbation method is considered. Further, the large  $\eta$  asymptotics is also performed. The model is reduced to a system of linear ordinary differential equations and solved in terms of confluent hypergeometric functions which are fully analyzed. The final §5 summarizes the discussion on the important results.



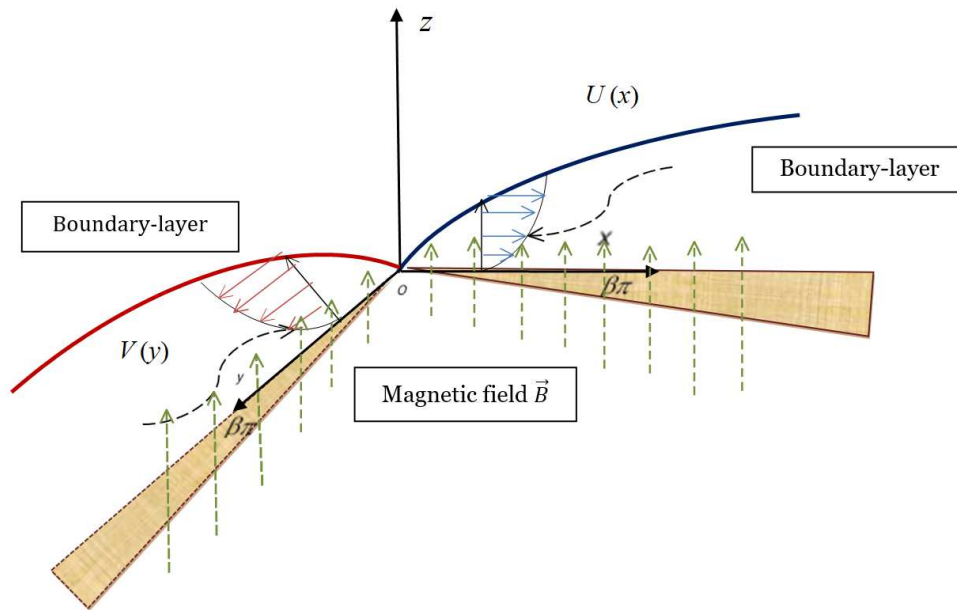


Fig. 1. A schematic configuration of the three-dimensional boundary-layer in presence of Magnetic field.

### 2. Flow Theory and Analysis

Consider a steady three-dimensional laminar viscous boundary-layer flow over a constant wedge in the presence of an electrically conducting fluid. We employ a system of Cartesian coordinates  $(x, y, z)$  in which  $x$ - and  $y$ - axes are measured (quite large) along the direction of the flow and  $z$ -axis is measured along normal to the flow, and the flow is in half-space  $z > 0$ . The fluid of viscosity  $\mu$  and constant density  $\rho$  is driven over the wedge surface in which the viscosity effects are confined to the boundary surface and away from the surface the flow is governed by the potential flow. The outer freestream velocities in both  $x$ - and  $y$ - directions are taken respectively  $U(x)$  and  $V(y)$  (these will be defined shortly) (see figure 1). Further, the magnetic field is applied normal to the flow (in the  $z$ -direction) in which an entire flow field is completely magnetized as shown in figure 1. The induced magnetic field produced by the motion of an electrically conducting fluid is almost negligible in comparison with the applied magnetic field since magnetic Reynolds number is very small i.e.  $R_m (= UL\sigma\mu_m) \ll 1$  where  $\mu_m$  is magnetic permeability and other variables will be defined later. It is assumed that no external electrical field is applied and the effect of polarization of the fluid is negligible. This is supported by the fact that the electrical energy is small compared to magnetic energy. We first give the Navier- Stokes equations for a viscous and incompressible fluid in the presence of applied magnetic field so that exact derivation of three-dimensional boundary-layer equations becomes simple. Thus, the continuity and momentum equations are

$$\nabla \cdot \vec{q} = 0, \tag{1}$$

$$(\vec{q} \cdot \nabla)\vec{q} = -\frac{1}{\rho}\nabla p + \frac{\mu}{\rho}\nabla^2\vec{q} + \frac{1}{\rho}\vec{j} \times \vec{B} \tag{2}$$

where  $\vec{q} = (u, v, w)$  is velocity vector in  $x, y$  and  $z$ -directions,  $p$  is the pressure,  $\vec{j}$  is the current density and  $\vec{B}(0, 0, B_0)$  is the magnetic field applied in  $z$ -direction. The last term in (2) is the body force between applied magnetic field and the fluid motion and is called the Lorentz force. It is defined as

$$\vec{j} = \sigma[\vec{q} \times \vec{B}] \tag{3}$$

where  $\sigma$  is electrical conductivity of the fluid. Thus, the evaluation of the last term in (2) using (3), we obtain

$$\vec{j} \times \vec{B} = \sigma[-uB_0^2\hat{i} - vB_0^2\hat{j} + 0 \cdot \hat{k}]. \tag{4}$$

Further, for a large Reynolds number  $Re (= UL/\nu)$  (in usual notations) flow, the viscosity effects are confined to a thin layer near the boundary. Within this thin layer, very large velocity gradients exist, i.e. the velocity gradient increase from the zero at the surface to the inviscid flow at the edge of the boundary-layer and also  $|\frac{\partial u}{\partial x}|, |\frac{\partial u}{\partial y}| \ll |\frac{\partial u}{\partial z}|$  and  $|\frac{\partial v}{\partial x}|, |\frac{\partial v}{\partial y}| \ll |\frac{\partial v}{\partial z}|$ . Let  $\delta$  be the thickness of the boundary-layer, then we have that  $\delta \ll L$ , except at the onset of the boundary-layer, where  $L$  is some reference length scale defined in the spatial direction. The velocity components  $(u, v, w)$  are non-dimensionalized with respect to the mainstream velocities  $U, V, W$ . We define the following independent dimensionless variables:

$$x^* = \frac{x}{L}, y^* = \frac{y}{L}, z^* = \frac{z}{\delta}, u^* = \frac{u}{U}, v^* = \frac{v}{V}, w^* = \frac{w}{W}, p^* = \frac{p}{P_\infty}$$

where  $\delta$  and  $P_\infty$  are certain reference quantities. With the above scaling and approximations, equations (1-4) can be written in boundary-layer form as (dropping superscript stars)

$$\frac{\partial u}{\partial x} + \frac{\partial v}{\partial y} + \frac{\partial w}{\partial z} = 0, \tag{5}$$



$$u \frac{\partial u}{\partial x} + v \frac{\partial u}{\partial y} + w \frac{\partial u}{\partial z} = -\frac{1}{\rho} \frac{\partial p}{\partial x} + \nu \frac{\partial^2 u}{\partial z^2} - \frac{\sigma B^2}{\rho} u, \quad (6)$$

$$u \frac{\partial v}{\partial x} + v \frac{\partial v}{\partial y} + w \frac{\partial v}{\partial z} = -\frac{1}{\rho} \frac{\partial p}{\partial y} + \nu \frac{\partial^2 v}{\partial z^2} - \frac{\sigma B^2}{\rho} v, \quad (7)$$

$$0 = \frac{\partial p}{\partial z} \quad (8)$$

where  $\nu$  represents the kinematic viscosity and is assumed constant. The pertinent boundary conditions are

$$\text{at } z = 0: u = v = w = 0, \text{ and as } z \rightarrow \infty: u \rightarrow U \quad \text{and} \quad v \rightarrow V \quad (9)$$

where  $U = U(x)$  and  $V = V(y)$  are velocity components in  $x$ - and  $y$ -directions outside the boundary-layer region. The above system (5-9) obviously restricts to the class of flows to be considered in the boundary-layer, however, the resulting class is significant from both theoretical as well as practical point of view. Also reduction of the above equations is fully rational i.e. all derivations can be justified on the basis of large Reynolds number theory, but we rather obtain Reynolds number independent solutions. Equation (8) shows that the normal pressure gradient is zero, i.e. the pressure is assumed uniform across the flow region. This means that an imposed pressure distribution in the potential flow is chosen to match exactly the pressure field of boundary-layer. This pressure gradient in the above system can be approximated from inviscid flow with  $u = U(x)$ , the momentum equation (6) becomes (Sowerby [1])

$$U \frac{dU}{dx} = -\frac{1}{\rho} \frac{\partial p}{\partial x} - \frac{\sigma B_z^2}{\rho} U. \quad (10a)$$

Similarly, with  $v = V(y)$  the momentum equation (7) becomes

$$V \frac{dV}{dy} = -\frac{1}{\rho} \frac{\partial p}{\partial y} - \frac{\sigma B_z^2}{\rho} V \quad (10b)$$

Following Batchelor [19], both potential flow velocities are expected to vary in a power-law manner with co-ordinate distance measured along the corresponding boundaries

$$U(x) = U_\infty x^m, \quad V(y) = V_\infty y^m \quad (11)$$

where  $U_\infty, V_\infty$  and  $m$  are constants. Here  $m$  defines the mainstream forcing on the boundary-layer in both directions (see (10)). When  $m$  is negative, the system has an adverse pressure gradient (i.e.  $\partial p / \partial x > 0$  and  $\partial p / \partial y > 0$ ) and for positive  $m$ , it has a favorable pressure gradient (i.e.  $\partial p / \partial x < 0$  and  $\partial p / \partial y < 0$ ). From (6), (7) and (10) we have

$$u \frac{\partial u}{\partial x} + v \frac{\partial u}{\partial y} + w \frac{\partial u}{\partial z} = U \frac{dU}{dx} + \nu \frac{\partial^2 u}{\partial z^2} - \frac{\sigma B^2}{\rho} (u - U), \quad (12)$$

$$u \frac{\partial v}{\partial x} + v \frac{\partial v}{\partial y} + w \frac{\partial v}{\partial z} = V \frac{dV}{dy} + \nu \frac{\partial^2 v}{\partial z^2} - \frac{\sigma B^2}{\rho} (v - V). \quad (13)$$

The components (dependent variables) in (12) and (13) can easily be reduced by introducing two unknown stream functions  $\psi_1$  and  $\psi_2$ , and defining them in the form

$$(u, v, w) = \left( \frac{\partial \psi_1}{\partial z}, \frac{\partial \psi_2}{\partial z}, -\left( \frac{\partial \psi_1}{\partial x} + \frac{\partial \psi_2}{\partial y} \right) \right) \quad (14)$$

which satisfy the continuity equation identically, and the momentum equations (12) and (13) become

$$\frac{\partial \psi_1}{\partial z} \frac{\partial^2 \psi_1}{\partial x \partial z} + \frac{\partial \psi_2}{\partial z} \frac{\partial^2 \psi_1}{\partial y \partial z} - \left( \frac{\partial \psi_1}{\partial x} + \frac{\partial \psi_2}{\partial y} \right) \frac{\partial^2 \psi_1}{\partial z^2} = U \frac{dU}{dx} + \nu \frac{\partial^3 \psi_1}{\partial z^3} - \frac{\sigma B_z^2}{\rho} \left( \frac{\partial \psi_1}{\partial z} - U \right), \quad (15)$$

$$\frac{\partial \psi_1}{\partial z} \frac{\partial^2 \psi_2}{\partial x \partial z} + \frac{\partial \psi_2}{\partial z} \frac{\partial^2 \psi_2}{\partial y \partial z} - \left( \frac{\partial \psi_1}{\partial x} + \frac{\partial \psi_2}{\partial y} \right) \frac{\partial^2 \psi_2}{\partial z^2} = V \frac{dV}{dy} + \nu \frac{\partial^3 \psi_2}{\partial z^3} - \frac{\sigma B_z^2}{\rho} \left( \frac{\partial \psi_2}{\partial z} - V \right). \quad (16)$$

In a similar way, as discussed by Rosenhead [8] for a stagnation point ( $m=1$ ), the number of independent variables ( $x, y, z$ ) in (15) and (16) can be reduced to one in accordance with similarity transformations if we set

$$\eta = \left( \frac{(m+1)U}{2\nu x} \right)^{\frac{1}{2}} z. \quad (17a)$$

The above similarity variable  $\eta$  helps to determine stream functions  $\psi_1$  and  $\psi_2$  in terms of new functions  $f(\eta)$  and  $g(\eta)$ . See the appendix for details on the stream functions. We set  $u/U = F(\eta)$ ,  $v/V = G(\eta)$  and making use of the above stream function  $u = \partial \psi_1 / \partial z$  in (14) and integrating it with respect to  $\eta$ , we get



$$\psi_1 = \left(\frac{2vxU}{m+1}\right)^{\frac{1}{2}} f(\eta) \tag{17b}$$

where  $f(\eta) = \int F(\eta)d\eta$ . Similarly, we get another stream function

$$\psi_2 = \left(\frac{2vy\alpha V}{m+1}\right)^{\frac{1}{2}} g(\eta) \tag{17c}$$

where  $g(\eta) = \int G(\eta)d\eta$ . This new set of transformations generally offers some advantages over the previous system (15-16) as it is beneficial to work with the  $\eta$ - differentiated form of (15-16). Substituting (17) in (15) and (16) we get a system of third order nonlinear ordinary differential equations

$$f''' + f''(f + \alpha\beta g) + \beta(1 - f'^2) - M^2(f' - 1) = 0, \tag{18a}$$

$$g''' + g''(f + \alpha\beta g) + \alpha\beta(1 - g'^2) - M^2(g' - 1) = 0, \tag{18b}$$

and the corresponding boundary conditions (9) become

$$f(0) = 0, f'(0) = 0, f'(\infty) = 1, \tag{18c}$$

$$g(0) = 0, g'(0) = 0, g'(\infty) = 1. \tag{18d}$$

where  $f = f(\eta), g = g(\eta)$  and  $\beta = 2m / (m + 1)$  is pressure gradient parameter,  $M^2 = 2\sigma L B_z^2 / ((m + 1)\rho U)$  is the Hartmann number which is the ratio of electromagnetic force to the viscous force in the boundary layer,  $\alpha = Vx / Uy$  is the shear-to-strain-rate parameter. Note that both  $f(\eta)$  and  $g(\eta)$  in (18) are functions of  $x$  and  $y$  (see (17)), however, Benzi et al. [20], [21] have proved that if  $x$  and  $y$  are replaced by  $L$  in the final equations, then dependence of  $x$  and  $y$  in (18) can easily be removed. Thus,  $\alpha = V_\infty / U_\infty$ . This approximation is justified in the boundary-layer approximation since the spatial direction length  $L$  is quite large, and also  $\partial_z \gg (\partial_x, \partial_y)$ . Further, if we interchange  $x$  and  $y$  in (17) then  $f(\eta)$  and  $g(\eta)$  will get interchanged in (18) which will not alter the physics of the problem. System (18) has been derived for the first time which describes the three-dimensional boundary layer flow of a viscous incompressible fluid in the presence of applied magnetic field with variable pressure gradient. The solutions of system of differential equations encompass wide variety of boundary layer flows including the standard two-dimensional classical boundary layer flows for some parameters. The last two derivative boundary conditions in (18c-18d) are such that both stream wise velocities approach the main stream flows as  $\eta \rightarrow \infty$  (i.e,  $\eta \rightarrow \eta_\infty$ , where  $\eta_\infty$  is large, is utilized explicitly in our calculations). Further, we define when  $\beta > 0$  the system has a favorable pressure gradient while for  $\beta < 0$  it has an adverse pressure gradient. The effects of pressure gradient shall be described later. In absence of magnetic field ( $M=0$ ), Howarth [22] reported solution of (18) in the range  $0 \leq \alpha \leq 1$ , and Davey [3] showed that similarity solutions exist for the system (18) in the range  $-1 \leq \alpha \leq 0$  for the case of stagnation point flow ( $\beta = 1$ ). We anticipate that the presence of magnetic field in the boundary-layer flow would modify this range of values of  $\alpha$  for which the velocity profiles in both directions exist.

Once similarity solutions to the problem exist for  $\beta, \alpha$  and  $M$ , these, in fact, are exact solutions of the Navier-Stokes equations in the boundary layer limit  $\delta \ll L$ . While quantitative solutions can be expected only for those physical parameters neither too small nor too large, the predictions would capture many important features of boundary layer flow such as flow oscillations, flow separations, etc. An equivalent asymptotic model for large  $\alpha$  will also be performed to support these numerical solutions.

When  $\alpha = 0$  and  $M = 0$ , both solutions are similar and are the two-dimensional classical Falkner-Skan boundary-layer flow (Rosenhead [8]) whilst for other values of  $\alpha$  and  $M$ , the full three-dimensional nonlinear differential equations may be studied by considering the effects variable pressure gradient, which is not carried out in the literature. In the light of above considerations, we now study direct numerical solution of the system (18).

### 3. Numerical Solution

Coupled nonlinear system (18) is numerically integrated across the boundary layer region using implicit finite-difference scheme. We discretize an entire flow domain with a very small grid size, and use the Keller-box solution method for the system (18) that consists of several steps. The two third-order differential equations (total order is six) is converted to the system of six first-order equations by introducing some additional unknowns. This first-order system is discretized with help of central finite-difference scheme which is second order accurate. This discretization produces nonlinear algebraic equations that are linearized via Newton's linearization technique. Once the system is linearized, we use the factorization method to solve the linear system and update the correction at each iteration until we obtain the convergent solution. In all our simulations, the error tolerance was set to  $10^{-8}$ . Our code adopts a variable grid-size and different flow domains to get the precise wall stress values  $f''(0)$  and  $g''(0)$ . The Keller-box solver works well and can be adjusted by adopting a very fine grid in the flow domain in order to capture any significant flow variations (Cebeci and Bradsha [23]). Once the solutions have been determined, the two-dimensional boundary-layer displacement thicknesses  $\delta_x$  and  $\delta_y$  may be calculated from the following relations

$$\int_0^\infty (1 - f'(\eta))d\eta = \delta_x, \int_0^\infty (1 - g'(\eta))d\eta = \delta_y. \tag{19}$$

Also of interest is the wall shear stress

$$\tau = \mu \left[ \frac{\partial u}{\partial z} i + \frac{\partial v}{\partial z} j \right]_{z=0} = \mu \left( \frac{m+1}{2xv} \right)^{\frac{1}{2}} U^{\frac{3}{2}} [f''(0)i + \alpha g''(0)j] \tag{20}$$

in which  $i$  and  $j$  are unit vectors directed along  $x$ - and  $y$ - axes.

Two further points of detail are worth mentioning. First for the class of similar solutions when  $\alpha$  is held constant and both  $\beta$  and  $M$  are varied, it is found that there is always a rapid convergence of the numerical scheme. Convergence of numerical scheme is achieved at  $\eta_\infty \approx 5$ . Secondly, when  $\alpha$  is varied, though there is a fast convergence in the  $x$ - momentum, very slow convergence in the crossflow direction is found. This computation turns out to be more challenging and the slow convergence is associated with the Keller-box code which is unable to satisfy the end condition asymptotically; it took larger flow domain and



hence several numbers of iterations. The convergence is finally achieved only at  $\eta \geq 14$ . Therefore, the results of  $y$ -momentum are qualitatively different from  $x$ -momentum profiles and also from the former case (when  $\alpha$  is held constant). In contrast to the earlier range of value of  $\alpha$ , the Keller-box code gives the similarity Solution of the system (18) in the range  $-1 \leq \alpha < \infty$  for all possible values of  $\beta$  and  $M$ . This lower limit of  $\alpha$  is effectively a function of magnetic field  $M$  and pressure gradient  $\beta$  i.e.  $\alpha = \alpha(M, \beta)$ . As  $M$  increases the lower limit still decreases that makes existence of some more velocity profiles.

The first numerical comparisons for the streamwise component of wall shear-stress  $f''(0)$  and crossflow component of wall shear-stress  $g''(0)$  in three-dimensional boundary-layer system in the absence of applied magnetic field  $M=0$  are computed for the case of the stagnation point flow and are presented in table 1. Note that these results are in good agreement with those given in Rosenhead [8] and Davey [3] for the same value of  $\alpha$ . Since this case has been discussed previously by Rosenhead [8] and Davey [3], these results are no longer discussed in this paper, and these calculations serve as a benchmark for our further computations. Further, for pressure gradient  $\beta = 0.5$ , the values of stresses  $f''(0)$  and  $g''(0)$  are displayed in table 2 for various values of  $M$  and  $\alpha$ . Also for given magnetic field ( $M=1$ ), the values of the wall stresses  $f''(0)$  and  $g''(0)$  are displayed in table 3 for various values of pressure gradient  $\beta$  and  $\alpha$ . In each case the velocity profiles  $f'(\eta)$  and  $g'(\eta)$  exist in the boundary layer. Note that as stated above, the self-similar solutions do exist for some range of negative  $\alpha$  beyond -1 and as  $M$  increases this range further decreases. For example for  $M=3$ , the solutions exist in the range  $-6 \leq \alpha < \infty$  whereas for  $M=0$ , this range is  $-1 \leq \alpha < \infty$ . This is due to the viscous forces in  $y$ - the direction in the boundary-layer are dominating over the inertial forces in  $x$ -directions, hence the outer boundary condition would not be satisfied.

## 4. Asymptotics

### 4.1 Large $\alpha$ asymptotics

Here we consider the asymptotic analysis of the three-dimensional boundary-layer equations for large  $\alpha$ . The solution of the full three-dimensional problem faces a considerable computational task for large  $\alpha$ . As discussed the slow convergence before, the fast convergence of the numerical scheme can be expected only for the moderate values of  $\alpha$ , it is required to perform large  $\alpha$  asymptotics on the full three-dimensional boundary-layer system (18). Although the present asymptotic analysis is qualitatively similar to the work of Weidman [5], there remains a huge numerical task because the system is still nonlinear and has applied magnetic force and pressure gradient effects. The asymptotic analysis for large  $\alpha$  is an alternative model that validates results obtained by the direct solution of the problem (18). Therefore, we pursue our analysis on the system (18) in the limit of large  $\alpha$ . This can be done by modifying  $f(\eta)$  and  $g(\eta)$  by incorporating large  $\alpha$  as

$$f(\eta) = \frac{F(\xi)}{\sqrt{\alpha}}, g(\eta) = \frac{G(\xi)}{\sqrt{\alpha}}, M^* = \frac{M}{\sqrt{\alpha}}, \xi = \sqrt{\alpha}\eta. \quad (21)$$

In this ansatz, since the uniform magnetic field is applied in the normal direction to the flow field, we can always modify our definition of  $M$  by a factor of  $\sqrt{\alpha}$  to get the same magnetic force in the system (18). With the new transformations (21), the system (18) can be written as

$$F''' + \left(\frac{F}{\alpha} + \beta G\right)F'' + \frac{\beta}{\alpha}(1 - F'^2) - M^{*2}(F' - 1) = 0, \quad (22a)$$

$$G''' + \left(\frac{F}{\alpha} + \beta G\right)G'' + \beta(1 - G'^2) - M^{*2}(G' - 1) = 0, \quad (22b)$$

where all derivatives are with respect to  $\xi$ . Because  $1/\sqrt{\alpha} \ll 1$ , it is appropriate to make use of the regular perturbation expansions in the system (22) as

$$F(\xi) = F_0(\xi) + (1/\alpha)F_1(\xi) + (1/\alpha^2)F_2(\xi) + \dots \quad (23a)$$

$$G(\xi) = G_0(\xi) + (1/\alpha)G_1(\xi) + (1/\alpha^2)G_2(\xi) + \dots \quad (23b)$$

for which a series of boundary value problems emerges at increasing order of  $1/\sqrt{\alpha}$ . The zeroth order system is given by

$$F_0''' + \beta G_0 F_0'' - M^{*2}(F_0' - 1) = 0, \quad (24a)$$

$$G_0''' + \beta G_0 G_0'' + \beta(1 - G_0'^2) - M^{*2}(G_0' - 1) = 0, \quad (24b)$$

$$F_0(0) = G_0(0) = 0, F_0'(\infty) = G_0'(\infty) = 0, F_0'(\infty) = G_0'(\infty) = 1. \quad (24c)$$

The above system (24) also captures the structure of three-dimensional viscous boundary layer in a steady flow. Again, we use the Keller-box code that has been described earlier for the solution of the nonlinear system (24) for all value of  $\beta$  and  $M$ . The shear stress parameters for  $\alpha \gg 1$  for different values of  $\beta$  and  $M$  are given by

$$f''(0) = \sqrt{\alpha}F_0''(0), g''(0) = \sqrt{\alpha}G_0''(0) \quad (25)$$

Note that these values increase unboundedly as  $\alpha \rightarrow \infty$ . Further, the displacement thicknesses

$$\delta_x \sim \frac{\delta_{x0}}{\sqrt{\alpha}}, \delta_y \sim \frac{\delta_{y0}}{\sqrt{\alpha}} \quad (26)$$

where

$$\delta_{x0} = \int_0^\infty (1 - F_0'(\xi))d\xi, \quad \delta_{y0} = \int_0^\infty (1 - G_0'(\xi))d\xi \quad (27)$$

are leading-order displacement thicknesses and are obtained by a numerical integration. The recent interesting work of Weidman [5] also gives equally valid, related displacement thicknesses, yet are derived from different similarity variables, but all lead to the same physical mechanisms. These results will be discussed shortly.



4.2 Far-field behavior

In this section, we study the development of the flow far-away from the surface in which the velocity profiles become linear as  $\eta \rightarrow \infty$  i.e.,  $|f'(\eta) - 1| \ll 1$  and  $|g'(\eta) - 1| \ll 1$  as  $\eta \rightarrow \infty$ . We will study the far-field behavior on general three-dimensional boundary layer flows possessing similar velocity profiles. Nonetheless, as discussed in the previous section, as such there is no condition on the physical parameters (i.e. on  $\alpha, \beta, M$ ), we, therefore, seek linearized solutions to the similarity problem by defining

$$f(\eta) = \eta + \delta_x + \int E(\eta)d\eta, g(\eta) = \eta + \delta_y + \int H(\eta)d\eta \tag{28}$$

where  $\delta_x$  and  $\delta_y$  are integration constants, in this case, obtained by the displacement thicknesses,  $E(\eta)$  and  $H(\eta)$  and their derivatives are assumed small. Substitution of (28) and its derivatives into (18) and upon linearization gives

$$E'' + (1 + \alpha\beta)(\delta_{xy} + \eta)E' - (2\beta + M^2)E = 0, \tag{29a}$$

$$H'' + (1 + \alpha\beta)(\delta_{xy} + \eta)H' - (2\alpha\beta + M^2)H = 0 \tag{29b}$$

and the corresponding boundary conditions then become

$$E(0) = -1, \quad E(\infty) = 0, \tag{29c}$$

$$H(0) = -1, \quad H(\infty) = 0, \tag{29d}$$

where the three-dimensional displacement thickness  $\delta_{xy}$  is given by

$$\delta_{xy} = \frac{\delta_x + \alpha\beta\delta_y}{1 + \alpha\beta}. \tag{30}$$

It is worth pointing out that the inclusion of  $\delta_x$  and  $\delta_y$  inevitably results in three-dimensional displacement thickness  $\delta_{xy}$ . Also in the special case of  $\alpha = 1$ , again the linearized system becomes identical ( $E \equiv H$ ), the flow thereby remains two-dimensional, and  $\delta_{xy} = \delta_y$  (or  $\delta_x$ ). In the work on two-dimensional boundary layer flow, Kudenatti *et al.* [24] considered a similar form that amounts to the system (29) with  $\delta_{xy} (= \delta_x)$  replaced by the mass transfer term. Further, a general discussion on the other values of  $\alpha$  shall be made later. Now note that the sign of  $\alpha$  and  $\beta$  plays a vital role in (29). Consider the first particular case when  $\alpha\beta = -1$  for which the linearized system (29) renders a good deal of simplification and hence the solutions of (29) that satisfy the boundary conditions in (29c) and (29d) are

$$E(\eta) = -e^{-\sqrt{2\beta+M^2}\eta}, \quad H(\eta) = -e^{-\sqrt{-2+M^2}\eta}. \tag{31}$$

The above solutions are such that the arguments under square root should be positive. On the other hand, when  $\alpha\beta \neq -1$ , the complete solution of the system (29) (partially obtained by Kudenatti *et al.* [25] for the two dimensional flow when  $\alpha = 0$ ) for all value of  $\alpha, \beta$  and  $M$  are expressed in terms of the Kummer function  $\mathcal{M}(\cdot, \cdot, \eta)$  and note that both solutions are similar except a small change in the first argument of the Kummer functions Abramowitz and Stegun [26] and Andrews [27] i.e.,

$$E(\eta) = H(\eta) = C_{1,2}\sqrt{k_1}(\eta + \delta_{xy}) \mathcal{M}\left(\frac{3}{2} - K_{1,2}, \frac{3}{2}, -k_1(\eta + \delta_{xy})^2\right) + D_{1,2}\mathcal{M}\left(1 - K_{1,2}, \frac{1}{2}, -k_1(\eta + \delta_{xy})^2\right) \tag{32}$$

where

$$C_{1,2} = \frac{k_2}{A_{1,2}}, \quad D_{1,2} = -\frac{1}{A_{1,2}}, A_{1,2} = \frac{-1}{dr},$$

$$dr = \sqrt{k_1 k_2} \mathcal{M}\left(\frac{3}{2} - K_{1,2}, \frac{3}{2}, -k_1 \delta_{xy}^2\right) - \mathcal{M}\left(1 - K_{1,2}, \frac{1}{2}, -k_1 \delta_{xy}^2\right),$$

$$k_1 = \frac{1 + \alpha\beta}{2}, \quad k_2 = \frac{2\Gamma(K_{1,2})}{\Gamma(K_{1,2} - \frac{1}{2})},$$

$$K_1 = \frac{1 + M^2 + 2\beta + 2\alpha\beta}{2(1 + \alpha\beta)}, \quad K_2 = \frac{2 + M^2 + 4\alpha\beta}{2(1 + \alpha\beta)}.$$

Note that the first and second suffixes in  $A_{1,2}, C_{1,2}, D_{1,2}, K_{1,2}$  denote the solution for  $E(\eta)$  and  $H(\eta)$  respectively. The velocity profiles  $f'(\eta)$  and  $g'(\eta)$  from (28) with (32) exist for all physical parameters involved in. Also, the asymptotic dependence of the solution (32) on parameters can be obtained further by taking  $\eta \rightarrow \infty$  as

$$E(Z) = H(Z) \sim Z^{K_{1,2}-1} \sqrt{\pi} \left[ \frac{C_{1,2} e^{\pm i\pi(\frac{3}{2}-K_{1,2})}}{2\Gamma(K_{1,2})} + \frac{D_{1,2} e^{\pm i\pi(1-K_{1,2})}}{\Gamma(K_{1,2} - \frac{1}{2})} \right] + e^{-Z} Z^{\frac{1}{2}-K_{1,2}} \sqrt{\pi} \left[ \frac{C_{1,2}}{2\Gamma(\frac{3}{2} - K_{1,2})} + \frac{D_{1,2}}{\Gamma(1 - K_{1,2})} \right], \tag{33}$$



where  $Z = \sqrt{k_1(\eta + \delta_{xy})^2}$ . The above equation (33) can be rewritten as

$$E(Z) = H(Z) \sim AZ^{\frac{1}{2}-K_{1,2}} e^{-Z} + BZ^{K_{1,2}-1} \quad (34)$$

where  $A$  and  $B$  are constants taken appropriately from equation (33). All the computations were performed for values of  $\alpha, \beta, M$  except for  $\alpha\beta = -1$ , and these all ultimately reverted to boundary-layer flow type. Thus, a close inspection of linearized system (29) and its solutions (31-32) reveals that an inviscid mechanism is predominant (since  $\eta \rightarrow \infty$ ), and the solutions are additional corrections to the main solutions (28). The simplified form (34) of (32) is always decaying solutions as  $\eta \rightarrow \infty$ .

## 5. Results and Discussion

In this paper, we have discovered a new class of solutions of three-dimensional boundary-layer flow in the presence of the applied magnetic field, and these solutions entirely depend on the pressure gradient and applied the magnetic field. The mainstream flows are approximated by the power-law relations (as a power of distance manner) in each direction. When we apply the same magnetic force on three-dimensional boundary-layer along with the same pressure gradient, both  $x$ - and  $y$ - momentum possess a very different behavior. Inside the boundary-layer, the governing nonlinear ordinary differential equations have been derived for the first time, and are solved numerically using the second order accurate Keller-box method. This method is extensively used to obtain similar solutions (velocity profiles, wall shear stresses, etc), in spite of severe numerical difficulties. Although the Keller-box takes a considerable finer grid especially for those with reverse flows, it did not encounter numerical instability problems. Particularly, when  $\alpha$  is decreased marginally from 0,  $y$ - momentum has reverse flow, and method took large flow domain to converge into the mainstream flow. For certain range of  $\alpha$  in which numerical convergence was often slow, an asymptotic analysis for large  $\alpha$  is also carried out.

There is now much evidence that the applied magnetic force can provoke significant responses inside the boundary-layer. Also with growing industrial applications of MHD (discussed previously), it is important to consider the effects of the magnetic field into the model, and hence the present results also encompass the various effects of magnetic (Hartmann) number on the three-dimensional boundary-layer flow. The occurrence of the main solution branch for all values of  $\alpha$  and  $\beta$  for given  $M$  includes two special cases (Howarth [22] for  $0 \leq \alpha \leq 1$ ; Davey [3] for  $-1 \leq \alpha$ , for  $\beta = 1$  and  $M = 0$ ) which serve benchmark for our all simulations along with a very special case of  $\alpha = 0$  permits much simplification in the problem reducing it to two-dimensional case. Therefore, our analysis embeds the aforementioned special cases, and indeed gives the solutions for other  $\alpha$ ,  $\beta$  and  $M$  as was a key feature of this study.

The difference between the magnetic and non-magnetic flow illustrates the significant qualitative behaviors on the velocity profiles when  $M$  is varied from zero. This influence is shown in figure 2 for different  $M$  and other parameters are kept constant. The numerical simulations of the three-dimensional boundary-layer flow using the Keller-box method yielded a rapid convergence and a small computational domain. When the flow starts under the influence of magnetic field, the boundary-layer is formed in both the directions and is mainly driven by the viscous effects. Computations at increasing  $M$  clearly indicate that the profiles becoming confined to the region close to the surface. As  $M$  increases, the system acquires more and more magnetization that makes boundary layers to confine to the wall surface. As a result, boundary-layer thickness decreases. The reason for this to happen is that when the magnetic field is applied, it releases more energy to the system that drives fluid faster. This, in turn, increases the Reynolds number and therefore the viscous effects are confined to the wedge surface so that vorticity is convected towards the wall. The prominent feature of thickening boundary layer is predominantly due to a viscous mechanism. In any case, the effects of magnetic field on the three-dimensional are relatively benign; thereby boundary layer separation is generally avoided.

On the other hand, figure 3 shows the similar velocity profiles  $f'(\eta)$  and  $g'(\eta)$  when the pressure gradient  $\beta$  is varied, and other parameters are held constant. For  $\beta$  small, both curves are directed towards the wall surface (small distance from the wall), whilst  $\beta$  increases further, both flows in the mainstream region just outside the boundary layers become entirely directed towards the wedge surface. In either case (figure 2 or 3) there does appear to be some correlation between magnetic field and pressure gradient which exhibits the similar velocity profiles and thickening boundary layer. In any case figures 2 and 3 show the velocity curves are well within the boundaries, did not show over-or-under shoots (oscillatory type flows). For increasing  $\beta$  or  $M$ , the numerical scheme converges to the outer flow at the same speed and takes a small distance from the wall surface.

Additionally, when  $\beta$  is taken to be negative (the adverse pressure gradient), other similarity solutions exist and are shown in figure 4. A very clear observation is that velocity profiles are no longer thin in contrast to  $\beta > 0$  results. These profiles are directed predominantly away from the wedge surface for decreasing  $\beta$ . Figure 4b is particularly appealing and rather challenging for two reasons: when adverse pressure gradient is negative and increases, the flow starts to show the reverse flow near the wall in  $y$ -momentum; also in the numerical code (the Keller-box),  $\eta_\infty$  is quite large ( $\eta_\infty \approx 25$ ) only at which the final condition is satisfied. In the former case, adverse pressure gradient surpasses the viscosity effects, as a result reverse flow occurs, and reattachment takes place away from the surface. There is, however, no qualitative change in  $x$ -momentum velocity profiles except thinning of the wall layers (compared with  $\beta > 0$  results).

When the pressure gradient  $\beta (> 0)$  and magnetic number  $M$  are held constant, figure 5 illustrates the velocity distributions  $f'(\eta)$  and  $g'(\eta)$  for various values of  $\alpha$  in the range  $(-3, 3)$ . About the constraint on the range of  $\alpha$  will be discussed later. These profiles explicate that, in contrast to the earlier profiles, numerical scheme converges much faster in the  $x$ - momentum (figure 5a) than the  $y$ - momentum (figure 5b). The former results are qualitatively similar to the previous set of profiles (as is for  $\beta$  and  $M$ ), but the latter results are rather interesting and significantly alters the flow phenomenon. For positive  $\alpha$  the flow is accelerated as is the case of  $\beta > 0$  or  $M$ , and for negative  $\alpha$  the flow is inevitably decelerated (like  $\beta < 0$ ). As  $\alpha$  is increased towards negative infinity, the model shows the tendency of reverse flow ( $g'(\eta) < 0$ ), only after  $\alpha \leq -1$ . The reverse flow occurs quite regularly in the smaller region close to the wedge surface, but reattachment takes place away from the wall. When reverse flow occurs for which the wall shear stress  $g''(0)$  changes its sign from positive to negative. In the boundary-layer, the viscous effects are convected towards the mainstream, and this alters the outer boundary condition in  $y$ -direction clearly indicating a predominant inviscid mechanism. This is evident from the Keller-box numerical scheme which inevitably suffers the slow convergence and hence takes the large distance from the wedge surface to converge.



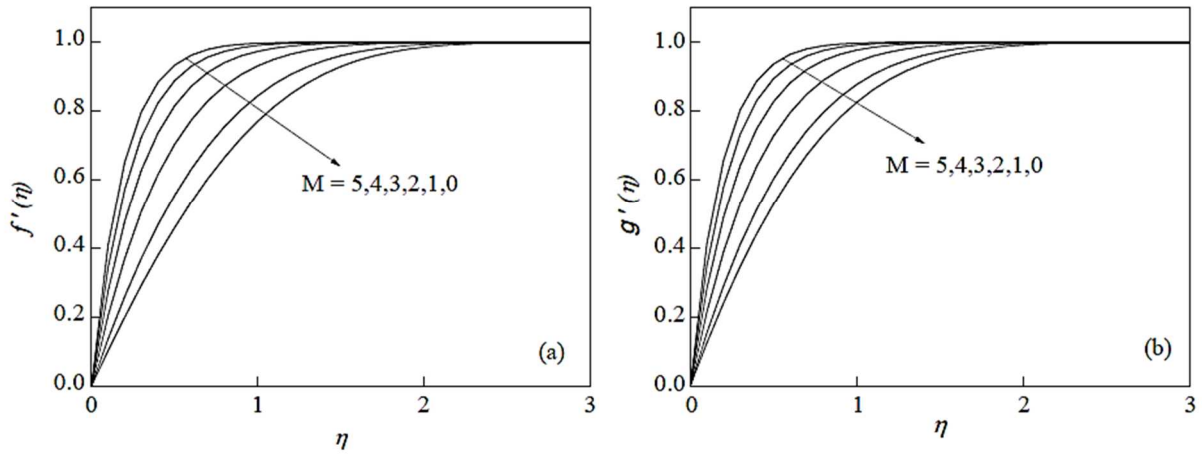


Fig. 2. Variation of velocity profiles  $f'(\eta)$  and  $g'(\eta)$  with  $\eta$  for different values of  $M$  keeping  $\beta = 0.5$  and  $\alpha = 2.0$  constant. There is as fast convergence of the profiles to their asymptotic condition for all values of  $M$  compared to  $M = 0$ .

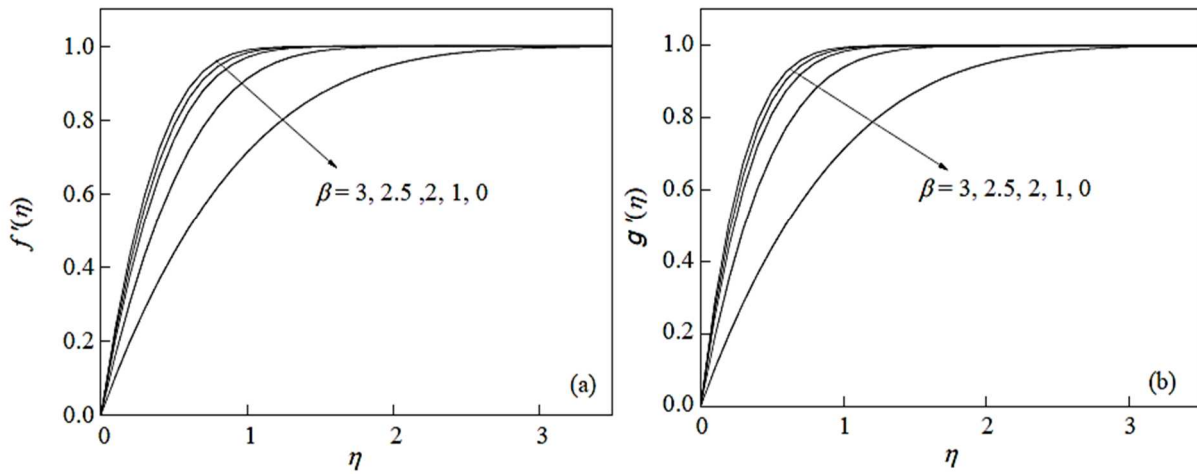


Fig. 3. Variation of velocity profiles  $f'(\eta)$  and  $g'(\eta)$  with  $\eta$  for different values of pressure gradient  $\beta$  and for  $M = 1.0$  and  $\alpha = 2.0$ . These simulations have been computed numerically from (18).

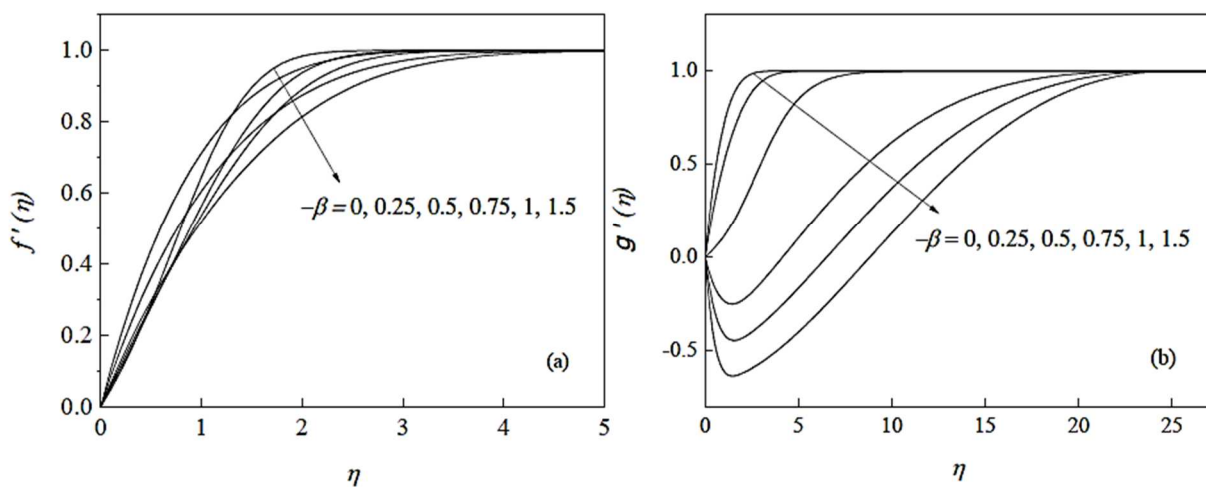


Fig. 4. Variation of velocity profiles  $f'(\eta)$  and  $g'(\eta)$  with  $\eta$  for different values of adverse pressure gradient  $\beta$  and for  $M = 1.0$  and  $\alpha = 2.0$ . These simulations have been computed numerically from (18).



Consequently, the code took several number of iterations to finally give the convergent solution although the scheme has faster convergence for  $x$ -momentum for the same set of parameters. This slow convergence is partly due to scatter of viscous effects near the edge of the boundary-layer. When  $\alpha$  is decreased beyond -3, no solution exists to the system (31) and (32) because the Keller-box code is unable to satisfy the outer boundary condition. Numerical computation corresponding to  $\alpha < -3$ , the three-dimensional MHD boundary-layer equations always yielded inconsistent results. Indeed, various techniques were performed; giving different initial conditions, small grid size, etc, to overcome this difficulty, but without success, and in all cases, the threshold value for not producing the similarity solutions was exactly found to occur at  $\alpha < -3$  when  $\beta = 0.5$ . When the pressure gradient is increased further, ( $\beta = 1$ ) the range for  $\alpha$  decreases i.e.,  $-1.5 \leq \alpha < \infty$ , this is evident from figure 6, for the same  $M = 1$ . Note that reverse flow occurs for smaller values of  $\alpha \in (-1, -1.5)$  in  $y$ -momentum and no solution exists beyond  $\alpha < -1.5$ . For  $\beta = 1$  and  $M=0$ , the results of Davey [3] who certainly reported three-dimensional solutions in the range  $-1 \leq \alpha \leq 0$ , have been recovered

Therefore, from our detailed numerical investigation on three-dimensional boundary-layer flow, two points are to be noted. First, whenever  $\beta$  values decrease towards negative infinity (from accelerated to decelerated), it was found that the range of  $\alpha$  also decreases towards negative infinity i.e.  $\alpha = \alpha(\beta)$ , and velocity profiles in  $x$ -momentum make the boundary layer thicker, whereas for  $y$ -momentum there is always boundary-layer separation for some  $\alpha$ . Secondly, the reverse flow is possible only for the cases  $M = 0$  (not discussed) and  $M = 1$ . We now anticipate that, when the application of magnetic field is increased (for example  $M \geq 2$ ), the flow is completely under the influence of magnetization, the boundary-layer separation naturally disappears in  $y$ -momentum, and makes boundary-layer thinner in both directions. In other words, the magnetic field actually controls and suppresses (or delays) the development of reverse flow in the boundary-layer. Simultaneously, the slow convergence problems associated with the Keller-box are also overcome thereby the convergence is achieved at the same speed in both directions, and also takes a smaller computational domain.

We now discuss all further three-dimensional results in terms of wall shear stresses  $f''(0)$  and  $g''(0)$  and displacement thicknesses  $\delta_x, \delta_y$  and  $\delta_{xy}$ . Note that in each case, the velocity profiles exist, and some discussion on class of flow and physical dynamics has been given before, but the present discussion does encompass various boundary-layer flows (including the two-dimensional). In particular, this discussion includes the following:

- i) Existence of wall shears  $f''(0)$  and  $g''(0)$ ;
- ii) Range of  $\alpha$  for which solutions exist;
- iii) Causes for limitation on  $\alpha$ .

To outline this, the Keller-box numerical solution of the system has been fully utilized, and wall shear stresses  $f''(0)$  and  $g''(0)$  are accordingly obtained. To supplement these results the large  $\alpha$  asymptotic has also been performed. For this asymptotic computation, the Keller-box code was developed, which is independent of  $\alpha$  to solve the system (24) and the code is less stringent compared to the original problem (18). The results of the asymptotic model are quantitatively similar to those obtained directly by the full system. To the author's knowledge, the asymptotic (large  $\alpha$ ) model has not been reported so far.

Both wall shear stresses ( $f''(0)$  and  $g''(0)$ ) results are plotted in figure 7 for various values of pressure gradient  $\beta (> 0)$  and for two sets of magnetic number ( $M = 1$  and  $M = 2$ ). Note that the solid lines represent the solutions obtained numerically by solving the full system (18) and the dashed lines are from the asymptotics (24). Both wall stresses are positive and grow unboundedly as  $\alpha$  increases. For small and negative  $\alpha$  the solutions do not exist. It can also be observed that there is a gradual increase in  $x$ -momentum wall stress (may be of the form algebraic) while  $g''(0)$  increases rapidly for all  $\beta$  investigated. In all positive  $\beta$  cases tested, the system shows a breakdown of the solution is found to occur at negative and small  $\alpha$ . In addition, these are validated by our large  $\alpha$  asymptotics which is shown by dashed lines and are plotted from  $\alpha \geq 3$ . This entire set of wall shear stresses ( $f''(0)$  and  $g''(0)$ ) is further convinced by solving three-dimensional boundary-layer equations for  $M = 2$  (figure 7b) for positive  $\beta$ . The system shows a very slight modification of the earlier results; thus we anticipate that the MHD three-dimensional model keeps this typical trend for all  $M$ . In any case, we did not observe reverse flow in both directions, and also velocity profiles converge to the mainstream at equal speed (although there are some exceptions).

The effects of the magnetic number  $M$  and pressure gradient  $\beta$  on the MHD three - dimensional boundary-layer solutions can be convincingly illustrated in tables 1 and 2 wherein the range of  $\alpha$  is clearly mentioned. For increasing  $\beta$ , the range of  $\alpha$  decreases, but for all positive  $\alpha$ , solutions continue to exist. As discussed in the previous section, when  $\beta$  is negative and increases, the solutions do exist and negative range of  $\alpha$  increases. However, from table 1, when  $M$  is increased predominantly, the solutions exist in the range  $(-\infty, \infty)$ . It is important to note that when  $\alpha = 1$ , both solutions of the three-dimensional boundary-layer coincide (i.e.  $f(\eta) = g(\eta)$  in (31)). This drastic modification on  $\alpha$  range is plausibly due to the term  $f + \alpha\beta g$  in the (31). These results in tables 1 and 2 and figures 7 and 8 clearly indicate that the system (31) always keeps the positive sign. That is to say that for both positive  $\alpha$  and  $\beta$ , the term  $f + \alpha\beta g$  becomes positive and there is a restriction on  $\alpha$  in negative side, and for both negative  $\alpha$  and  $\beta$ , the term  $f + \alpha\beta g$  still becomes positive and a restriction is on positive side. Another crucial note is that both  $\beta$  and  $\alpha$  are either  $+\beta$  and  $+\alpha$  or  $-\beta$  and  $-\alpha$ .

We now turn our attention to discuss the other solutions obtained for both positive and negative pressure gradient parameters. Particularly we discuss the clear restriction on  $\alpha$  for both positive and negative values of the pressure gradient. All the wall shear stresses ( $f''(0)$  and  $g''(0)$ ) are calculated exactly as before and are shown in figure 8 as a function of  $\alpha$  for various  $\beta$  and for  $M = 2$ . In this case, asymptotic solutions for large  $\alpha$  have not been shown in a figure 8 because there are negative  $\alpha$  results as well, although wall shear stresses are well comparable for positive  $\alpha$ . A close examination reveals that when ( $\beta < 0$  (or  $> 0$ )), the solutions to the problem exist for the range of  $\alpha \in (-\infty, \alpha_+)$  (or  $\alpha \in [\alpha_-, \infty)$ ) where  $\alpha_+$  and  $\alpha_-$  are respectively positive and negative threshold values of  $\alpha$  and are small enough. In fact, these are functions of  $\beta$  and  $M$ . For example, for  $\beta = -1.5$ , the threshold value  $\alpha_+$  of  $\alpha$  is +3 and as  $\beta$  increases from -1.5 to 1.5,  $\alpha_+$  changes its sign from positive to negative (becomes  $\alpha_-$ ). From our repeated calculations we surmise that there exists threshold values  $\alpha_+$  and  $\alpha_-$  of  $\alpha$  beyond which the solutions do not occur. In these calculations, the outer boundary conditions are never satisfied as viscosity effects may be dissipated towards the mainstream flow. Also, for  $\beta = 0$  in figure 8, surprisingly both solutions are similar and constant for all values of  $\alpha$ , and is shown it by thick horizontal straight line. The case  $\beta = 0$  corresponds to the flow over a flat plate. In all these cases,  $M = 2$  was held constant. We anticipate that when magnetic field is increased we expect that the solutions to the problem exist over entire range of  $\alpha$  i.e.  $\alpha \in (-\infty, \infty)$ , and boundary layer separations, computational challenges, etc., could be avoided.



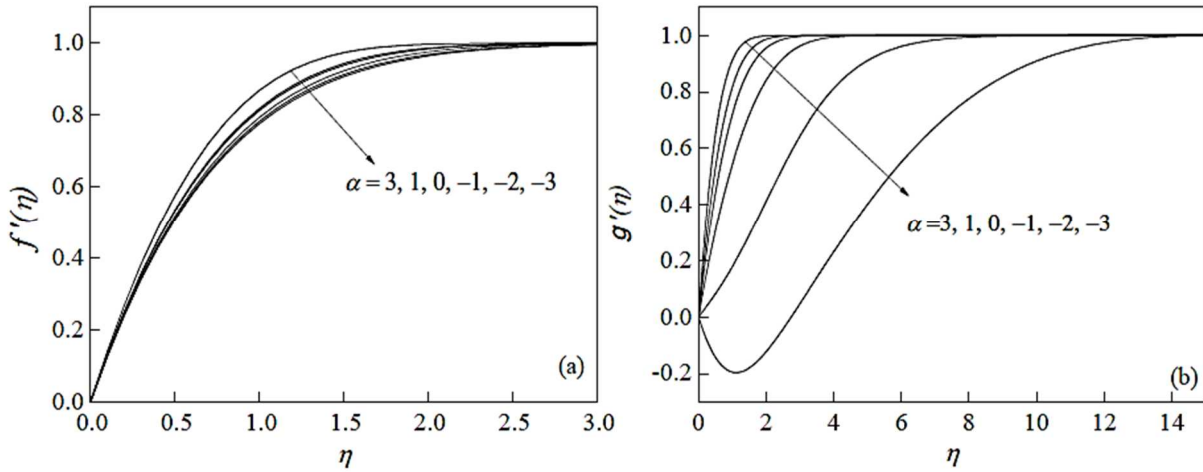


Fig. 5. Variation of velocity profiles  $f'(\eta)$  and  $g'(\eta)$  with  $\eta$  for various values of  $\alpha$  for magnetic number  $M = 1$  and pressure gradient  $\beta = 0.5$ . Note that we use Keller-box method for their simulations, their asymptotic approach is quite different. The curve for  $f'(\eta)$  approach their end-condition quite faster while the curve for  $g'(\eta)$  converge very slowly.

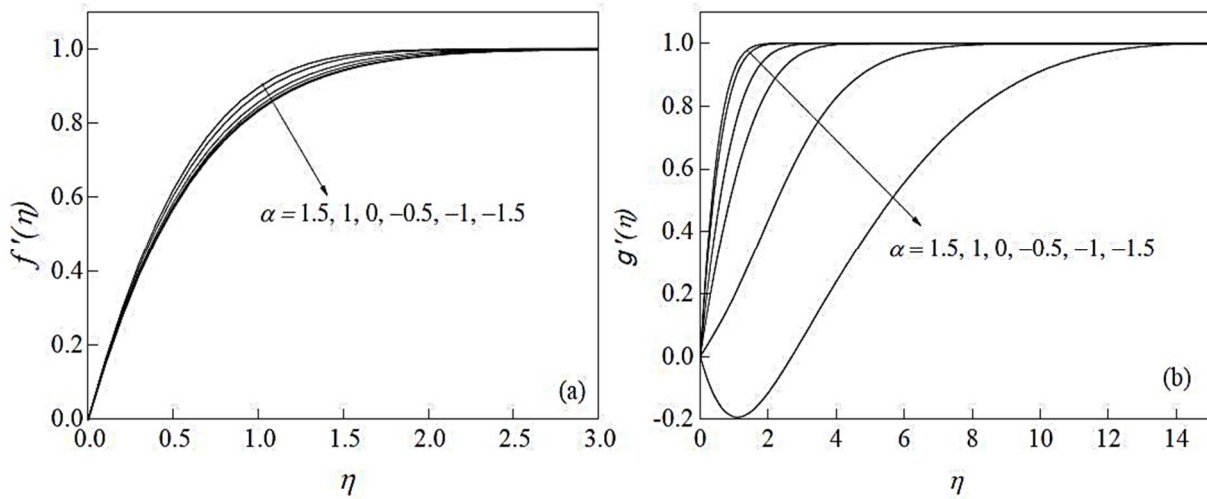


Fig. 6. Variation of velocity profiles for different values of  $\alpha$ ,  $M = 1$  and  $\beta = 1.0$ . These simulations have been performed using the equations (18) by Keller-box method.

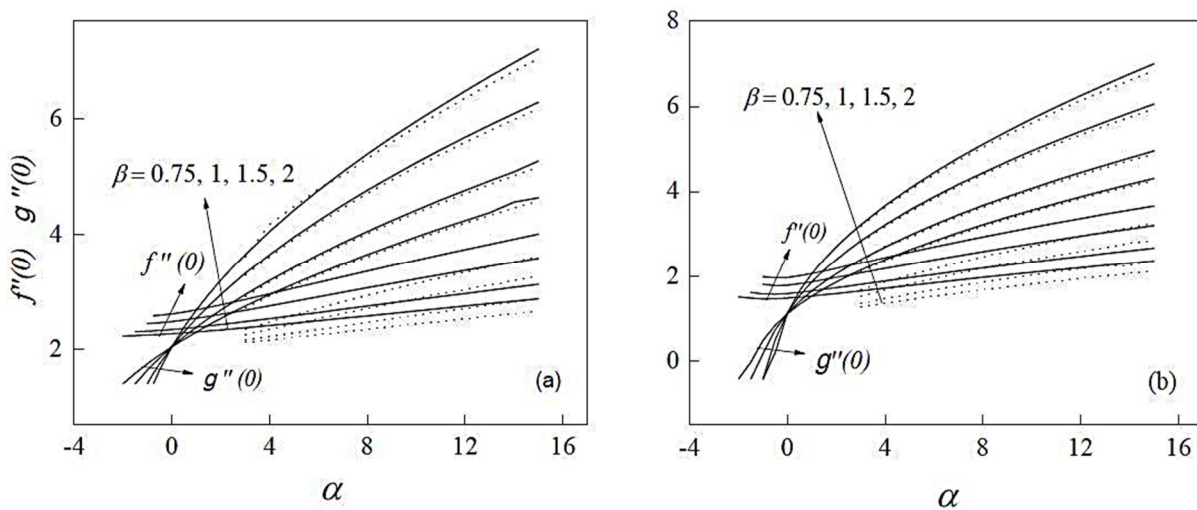


Fig. 7. Illustration of how both wall stresses vary with  $\alpha$  for different values of favorable pressure gradient  $\beta$  when (a)  $M = 1$  (b)  $M = 2$  are held constant. These are (solid lines) computed directly from the system (18), and the dashed lines are from the asymptotic solution (25).



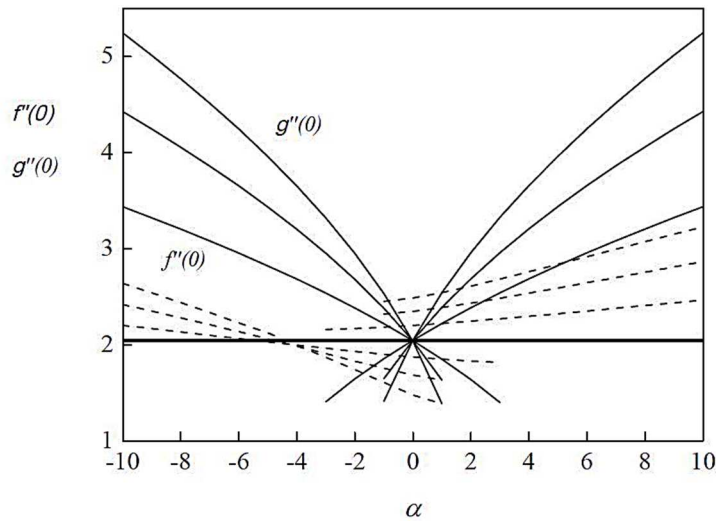


Fig. 8. Variation of the wall stresses value with  $\alpha$  for the  $\beta = -1.5, -1, -0.5, 0, 0.5, 1, 1.5$  and  $M = 2$ .

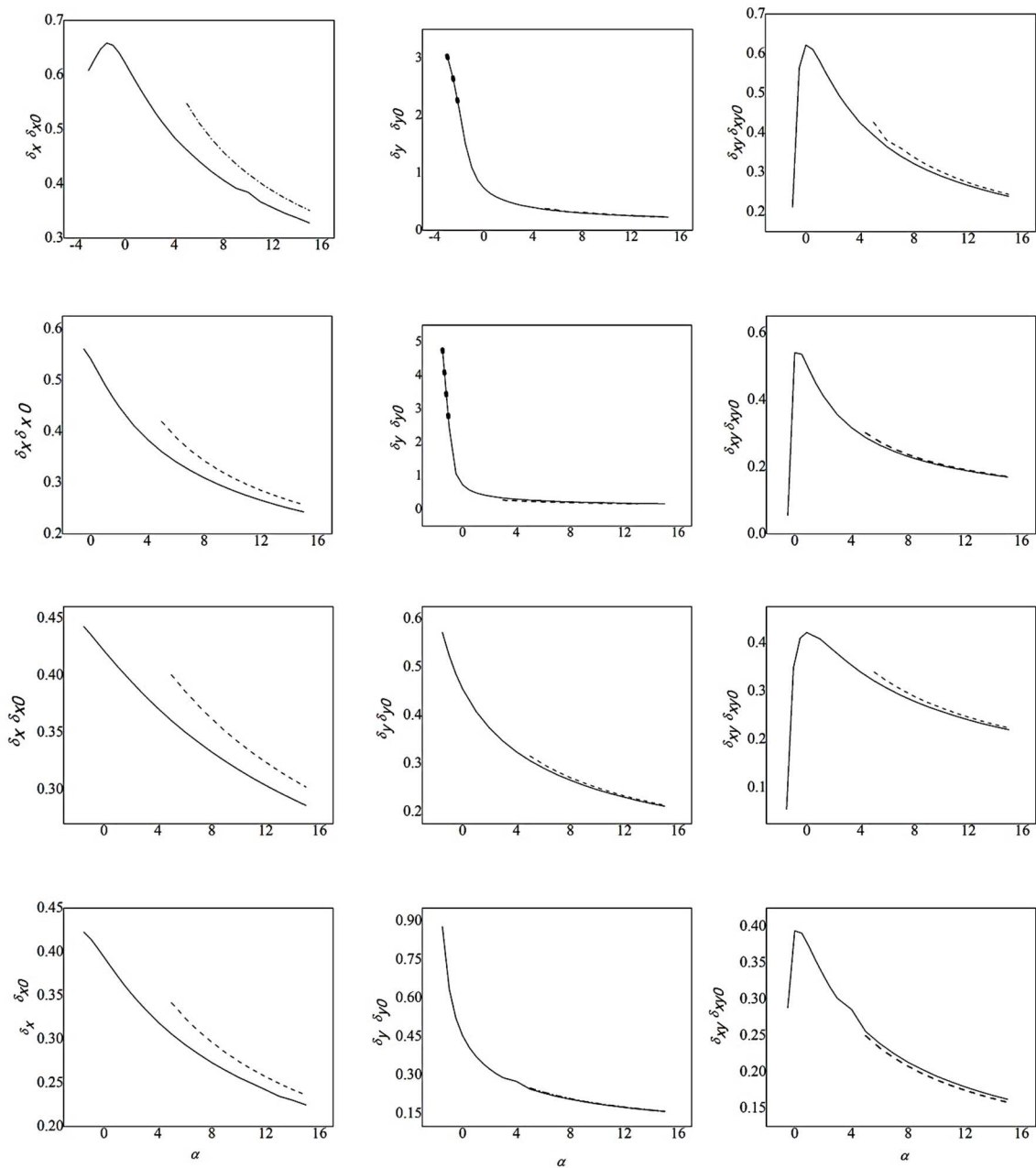


Fig. 9. Computation of the displacement thicknesses (solid lines) directly from (18) and asymptotically (dashed) from (25 and 26) for different values of  $M$  and  $\beta$  (first row for  $M = 1.0, \beta = 0.5$ , second row for  $M = 1.0, \beta = 1.0$  third row for  $M = 2.0, \beta = 0.5$ , fourth row for  $M = 2.0, \beta = 1.0$ ).



**Table 1.** Comparison of the skin-frictions  $f''(0)$  and  $g''(0)$  in both directions with existing solutions in the absence of magnetic field  $M = 0$  and for stagnation point flow  $\beta = 1$ .

$\alpha$	$f''(0)$ (Present)	$f''(0)$ (Davey)	$f''(0)$ (Rosen-head)	$g''(0)$ (Present)	$g''(0)$ (Davey)	$g''(0)$ (Rosen-head)
-1	1.27334821	1.2729	—	-0.8026247	-0.8112	—
-0.75	1.24845705	1.2473	—	-0.4830274	-0.4821	—
-0.5	1.23118058	1.2302	—	-0.1118225	-0.1115	—
-0.25	1.22603121	1.2251	—	0.26803122	0.2680	—
0	1.23358112	1.2326	1.233	0.57082486	0.5705	0.570
0.25	1.24875118	—	1.247	0.80582128	—	0.805
0.5	1.26820802	—	1.267	0.99912268	—	0.998
0.75	1.29018268	—	1.288	1.16570272	—	1.64
1	1.31373267	—	1.312	1.31373267	—	1.312

**Table 2.** The values of wall shear stresses  $f''(0)$  and  $g''(0)$  obtained by the numerical solutions of the system (18) for various values of  $\alpha$  and  $M$  when the pressure gradient  $\beta = 0.5$  is held constant. The down-marked arrows show the solutions of the system (18) continue to exist as  $\alpha$  increases.

$\alpha$	$M = 0$		$M = 1$		$M = 3$		$M = 5$	
	$f''(0)$	$g''(0)$	$f''(0)$	$g''(0)$	$f''(0)$	$g''(0)$	$f''(0)$	$g''(0)$
-15	—	—	—	—	—	—	4.97979	3.74295
-12	—	—	—	—	—	—	4.99499	4.02189
-9	—	—	—	—	—	—	5.01345	4.27915
-6	—	—	—	—	3.07523	2.17847	5.03486	4.54199
-3	—	—	1.39217	-0.42603	3.10066	2.63293	5.05891	4.78522
-1	1.27334	-0.80262	1.33816	0.72236	3.12441	2.90302	5.07626	4.94199
0.0	1.23358	0.57082	1.36068	1.10357	3.13796	3.03005	5.08532	5.01872
1	1.31373	1.31373	1.39668	1.39668	3.15245	3.15245	5.09457	5.09457
3	1.40564	1.80145	1.48399	1.85753	3.18386	3.38512	5.11378	5.24351
5	1.52621	2.02874	1.57704	2.22911	3.21791	3.60397	5.33877	5.38897
10	1.78542	2.52648	1.80522	2.96726	3.31124	4.10402	5.18709	5.73898
↓	↓	↓	↓	↓	↓	↓	↓	↓

At large  $\eta$  (far away from the wedge surface), in addition to direct numerical computations, the three-dimensional model provides a reliable means of flow phenomena including pressure gradient and magnetic field effects although it is a mere extension of the two-dimensional case of Kudenatti et al. [28] to the present analysis. The localized solutions (32) are the solutions of the original system (18) in the asymptotic limit of large  $\eta$  and are obviously resemble and interpret very much in the same way as in numerical solutions. Therefore, it is not our intention here to discuss the nature of the flow field. Rather we focus mainly on the three-dimensional displacement thickness  $\delta_{xy}$  given by (30). Note that, for  $\alpha = 1$ , the system (29) becomes  $E(\eta) \equiv H(\eta)$ , and accordingly  $\delta_x \equiv \delta_y$ , then (30) becomes  $\delta_{xy} = \delta_x$  or  $\delta_y$ .

Some of the displacement thicknesses for two- and three-dimensional flows are plotted in figure 9 for two sets of  $\beta$  and  $M$ . The numerical integrations to obtain  $\delta_x$  and  $\delta_y$  are performed and included as a part of the computation. The solid lines are plotted from (19) and (30) and dashed lines from asymptotic results (26) and (30) (in (30)  $\delta_x$  and  $\delta_y$  are replaced by  $\delta_{x0}$  and  $\delta_{y0}$ ). There is an excellent agreement between displacement thicknesses obtained from numerical solutions as well as from asymptotic for large  $\alpha$  and  $\eta$ . These clearly reveal that there is a gradual decrease in  $\delta_x$ ,  $\delta_y$  and  $\delta_{xy}$  as  $\alpha$  increases. This means that thickness of the boundary-layer becomes thinner as  $\alpha$  increases. However, in the case of three-dimensional displacement thickness  $\delta_{xy}$  increases first for some values of  $\alpha$  (near zero) and starts to decrease for increasing  $\alpha$ . These results are further supplemented by asymptotic results. Thick circles represent that there is a reverse flow in  $y$ -directions for these values of  $\alpha$ . The above results are true even for  $M = 2$ , perhaps reverse flow disappears and flow is ultimately convected towards the wedge surface. Indeed, similar computations were done for the higher magnetic field ( $M \geq 3$ ) but in all the cases the results were just analogues.

### 6. Concluding Remarks

In this paper, three-dimensional boundary-layer flow of a viscous fluid over an impermeable wedge in the presence of applied magnetic field has been studied with aid of Keller-box and asymptotic solution methods. The governing equations of motion are carefully solved and a detailed study of the flow parameters is obtained. The numerical solutions are further confirmed by the asymptotic results and a comprehensive quantitative analysis between two has been made. It is found that an excellent qualitative agreement between two results. It is observed that the wall shear stresses increase unboundedly for increasing  $\alpha$  from zero for  $\beta > 0$ . It is also noticed that there is a restriction on  $\alpha$  according to whether  $\beta$  is positive or negative. Nevertheless, this restriction on  $\alpha$  can be minimized with help of  $\beta$  and  $M$ . Taking appropriate values for  $\beta$  and  $M$ , the range of solution space on  $\alpha$  in the three-dimensional boundary-layer flow can be enhanced. The present numerical investigation reveals that these results are rather unusual for three-dimensional boundary-layer flow which have been not reported so far. The most important conclusion from the present numerical solution is that these flows are always attached to the wedge surface and are likely to be stable for accelerated flows and magnetic field. Thus two parameters further make the reverse flow to disappear from the boundary-layer flow by eliminating the decelerated fluid particles. Thus, the boundary-layer thickness in both directions becomes thinner for increasing  $\beta$  and  $M$ . When  $\alpha$  is taken to be negative the reverse flow appears quite regularly, however, it can be delayed by increasing the magnetic field. The applied magnetic field always stabilizes the flow thereby making the velocity profiles benign.



**Table 3.** The values of wall shear stresses  $f''(0)$  and  $g''(0)$  obtained by the numerical solutions of the system (18) for various values of  $\alpha$  and pressure gradient  $\beta$  for fixed Hartmann number  $M = 1$ . The down-marked arrows show the solutions of the system (18) continue to exist as  $\alpha$  increases.

	$\beta = 0.75$		$\beta = 1$		$\beta = 1.5$		$\beta = 2$	
$A$	$f''(0)$	$g''(0)$	$f''(0)$	$g''(0)$	$f''(0)$	$g''(0)$	$f''(0)$	$g''(0)$
-2	1.50512	-0.42609	—	—	—	—	—	—
-1.5	1.47748	-0.03309	1.61060	-0.42609	—	—	—	—
-1.0	1.45768	0.47828	1.57669	0.17286	1.80397	-0.42606	—	—
-0.75	1.45759	0.67214	1.56881	0.48625	1.78408	-0.02558	1.97917	-0.42616
-0.5	1.46167	0.83682	1.56964	0.73648	1.77010	0.49899	1.95585	0.19130
0.0	1.47781	1.10851	1.58648	1.11285	1.78436	1.12013	1.96264	1.12606
1.0	1.52709	1.52709	1.64731	1.64731	1.86489	1.86489	2.05992	2.05992
3.0	1.64997	2.14358	1.80162	2.39655	2.07342	2.83746	2.31487	3.22043
5.0	1.77894	2.62417	1.96146	2.96868	2.28558	3.56253	2.57143	4.07456
10.0	2.08566	3.56124	2.33496	4.07336	2.77172	4.95025	3.15348	5.70439
↓	↓	↓	↓	↓	↓	↓	↓	↓

### Author Contributions

The manuscript was prepared by the contribution of all authors. R.B. Kudenatti initiated the work, planned the solution scheme and suggested the problem. S.S. Prabha Gogate developed the mathematical modeling and examined the theory validation. Both the authors analyzed the empirical results, reviewed and approved the final version of the manuscript.

### Acknowledgements

We thank anonymous reviewers for their useful comments which improved the manuscript.

### Conflict of Interest

We hereby declare that we do not have any conflict of interest.

### Funding

The authors received no financial support for the research, authorship, and publication of this article.

### Data Availability Statements

The datasets generated and/or analyzed during the current study are available from the corresponding author on reasonable request.

### References

- [1] SOWERBY, L. The three-dimensional laminar boundary-layer on a flat plate. *Journal of Fluid Mechanics*, 22, 1965, 587-598.
- [2] BANKS, W. H. H. A three-dimensional laminar boundary-layer calculation. *Journal of Fluid Mechanics*, 28, 1967, 769-792.
- [3] DAVEY, A. Boundary layer flow at a saddle point of attachment. *Journal of Fluid Mechanics*, 10, 1961, 593-610.
- [4] DAVEY, A. & SCHOFIELD, D. Three-dimensional flow near a two-dimensional stagnation point. *Journal of Fluid Mechanics*, 28, 1967, 149-151.
- [5] WEIDMAN, P. D. Non-axisymmetric Homann stagnation-point flows. *Journal of Fluid Mechanics*, 702, 2012, 460-469.
- [6] HIRSCHL, E. H., COUSTEIX, J. & KORADULLA, W. *Three-Dimensional Attached viscous flow*, Springer, 2014.
- [7] DUCK, P. W., STOW, S. R. & DHANAK, M. R. Boundary-layer flow along a ridge: alternatives to the Falkner-Skan solutions, *Philosophical Transactions of the Royal Society A*, 358, 2000, 3075-3090.
- [8] ROSENHEAD, L. *Laminar boundary layers*, Oxford, Eng., Clarendon Press, 1963.
- [9] DUCK, P. W. & DRY, S. L. On a class of unsteady, nonparallel, three-dimensional disturbances to boundary-layer flows, *Journal of Fluid Mechanics*, 441, 2001, 31-65.
- [10] HAYAT, T., NASEEM, A., FAROOQ, M. & ALSAEDI, A. Unsteady MHD three-dimensional flow with viscous dissipation and Joule heating, *The European Physical Journal Plus*, 2013, 128-158.
- [11] OSKAM, B. & VELDMAN, A. E. P. Branching of the Falkner-Skan solutions for  $\lambda < 0$ , *Journal of Engineering Mathematics*, 16, 1982, 295-308.
- [12] SOMMERIA, J. & MOREAU, R. Why, how, and when, MHD turbulence becomes two dimensional, *Journal of Fluid Mechanics*, 118, 1981, 507-518.
- [13] TAKHAR, H. S., CHAMKHA, A. J. & NATH, G. Unsteady three dimensional MHD boundary layer flow due to the impulsive motion of a stretching surface, *Acta Mechanica*, 146, 2001, 59-71.
- [14] HAYAT, T., QASIM, M. & ABBAS, Z. Homotopy solution for the unsteady three dimensional MHD flow and mass transfer in a porous space, *Communications in Nonlinear Science and Numerical Simulation*, 15, 2010, 2375-2387.
- [15] ISHAK, A., NAZAR, R., POP, I. MHD boundary-layer flow due to a moving extensible surface, *Journal of Engineering Mathematics*, 62, 2008, 23-33.
- [16] AWALUDIN, I.S., ISHAK, A., POP, I. On the stability of MHD Boundary layer flow over a stretching/shrinking wedge, *Sci. Rep.*, 8(1), 2018, 1-8.
- [17] SINGH, J., MAHABALESHWAR, U.S., BOGNAR, G. Mass transpiration in nonlinear MHD flow due to porous stretching sheet, *Sci. Rep.*, 9(1), 2019, 1-15.
- [18] KELLER, H. B. *A new difference scheme for parabolic problems, in numerical solutions of partial difference equations*, Academic Press, New York, 1970, 369-377.
- [19] BATCHELOR, G. K. *An introduction to fluid dynamics*, 1st edition, Cambridge University Press, 1967.
- [20] BENZI, R., CHING, E. S. C. & CHU, V. W. S. Heat transport by laminar boundary layer flow with polymers, *Journal of Fluid Mechanics*, 696, 2012, 330-344.
- [21] BENZI, R., CHING, E. S. C., YU, W. C. K. & WANG, Y. Heat transport modification by finitely extensible polymers in laminar boundary-layer flow, *Journal of Fluid Mechanics*, 788, 2016, 337-357.



[22] HOWARTH, L. Note on the boundary layers on a rotating sphere, *Phil. Magz.*, 1951, 1308-1315.  
 [23] CEBECI, T. & BRADSHAW, P. *Momentum transfer in boundary layers*, Mc.Graw Hill, New York, 1977.  
 [24] KUDENATTI, R. B., KIRSUR, S. R., ACHALA, L. N. & BUJURKE, N. M. MHD boundary layer flow over a non-linear stretching boundary with suction and injection, *International Journal of Non-linear Mechanics*, 50, 2013, 58-67.  
 [25] KUDENATTI, R. B., KIRSUR, S. R., ACHALA, L. N. & BUJURKE, N. M. Exact solution of two-dimensional MHD boundary layer flow over a semi-infinite flat plate, *Communications in Nonlinear Science and Numerical Simulation*, 18, 2013, 1151-1161.  
 [26] ABRAMOWITZ, M. & STEGUN, I. *Handbook of mathematical functions with formulas, graph and mathematical tables*, 9th edition, Dover Publications, 1970.  
 [27] ANDREWS, L. *Special functions of mathematics for engineers*, 2nd edition, Oxford University Press, 1988.  
 [28] KUDENATTI, R. B. & KIRSUR, S. R. Numerical and asymptotic study of nonaxisymmetric magnetohydrodynamic boundary layer stagnation-point flows, *Math. Meth. Appl. Sci.*, 40(16), 2017, 5841-5850.

### Appendix

We have followed the mathematical derivation given by Rosenhead ([8], pp. 463) for three-dimensional stagnation point flows. Accordingly, we define for wedge flows

$$\eta = \left(\frac{(m + 1)U}{2vx}\right)^{\frac{1}{2}} z, \tag{A1}$$

$$\psi_1 = \left(\frac{2vxU}{m+1}\right)^{\frac{1}{2}} f(\eta), \tag{A2}$$

$$\psi_2 = \left(\frac{2vy\alpha V}{m+1}\right)^{\frac{1}{2}} g(\eta). \tag{A3}$$

Suppose, we rewrite (A2) and (A3) as

$$\psi_1 = \left(\frac{2vxU}{(m + 1)U}\right)^{\frac{1}{2}} f(\eta) = \left(\frac{2vx}{(m + 1)U}\right)^{\frac{1}{2}} Uf(\eta) \tag{A4}$$

$$\psi_2 = \left(\frac{2vyVVx}{(m + 1)Uy}\right)^{\frac{1}{2}} g(\eta) = \left(\frac{2vx}{(m + 1)U}\right)^{\frac{1}{2}} Vg(\eta).$$

We now let  $u / U = F(\eta)$  and  $v / V = G(\eta)$ . Letting

$$u = \frac{\partial\psi_1}{\partial z} \tag{A5}$$

where  $\psi_1$  is the stream function. To obtain the stream function  $\psi_1$ , we integrate the above equation

$$\int d\psi_1 = \int u dz = \int UF(\eta) dz = \int UF(\eta) \sqrt{\frac{2vx}{(m + 1)U}} d\eta$$

which implies

$$\psi_1 = \int \sqrt{\frac{2vx}{(m + 1)U}} UF(\eta) d\eta = \sqrt{\frac{2vx}{(m + 1)U}} U \int F(\eta) d\eta, \quad \psi_1 = \sqrt{\frac{2vx}{(m + 1)U}} Uf(\eta). \tag{A6}$$

where  $f(\eta) = \int F(\eta) d\eta$ . Similarly, for other stream function

$$\psi_2 = \left(\frac{2vx}{(m + 1)U}\right)^{\frac{1}{2}} Vg(\eta). \tag{A7}$$

We thus get the similarity transformations defined in (17) and proceeded to obtain the system of nonlinear ordinary differential equations.

### ORCID iD

S. Shashi Prabha Gogate  <https://orcid.org/0000-0002-3729-5768>  
 Ramesh B. Kudenatti  <https://orcid.org/0000-0002-4338-947X>



© 2022 Shahid Chamran University of Ahvaz, Ahvaz, Iran. This article is an open access article distributed under the terms and conditions of the Creative Commons Attribution-NonCommercial 4.0 International (CC BY-NC 4.0 license) (<http://creativecommons.org/licenses/by-nc/4.0/>).

**How to cite this article:** Prabha Gogate S.S., Kudenatti R.B. Numerical Study of Three-dimensional Boundary-layer Flow over a Wedge: Magnetic Field Analysis, *J. Appl. Comput. Mech.*, 8(3), 2022, 876–890. <https://doi.org/10.22055/JACM.2020.33142.2168>

**Publisher’s Note** Shahid Chamran University of Ahvaz remains neutral with regard to jurisdictional claims in published maps and institutional affiliations.

